Nano Research
2023, 16(12): 13283–13293

ISSN 1998-0124 CN 11-5974/O4
https://doi.org/10.1007/s12274-023-5921-6

Research Article

Glioblastoma cell-derived exosomes functionalized with peptides as efficient nanocarriers for synergistic chemotherapy of glioblastoma with improved biosafety

Ying Zhou[1,2,§], Long Wang[1,2,§], Lufei Chen[1,§], Wei Wu[1,§], Zhimin Yang[1,2], Yuanzhuo Wang[2,3], Anqi Wang[1,2], Sujun Jiang[1,2], Xuzhen Qin[4] (✉), Zucheng Ye[1] (✉), Zhiyuan Hu[1,2,3,5] (✉), and Zihua Wang[1,2] (✉)

[1] *Fujian Key Laboratory of Translational Research in Cancer and Neurodegenerative Diseases, Fujian Provincial Key Laboratory of Brain Aging and Neurodegenerative Diseases, School of Basic Medical Sciences, Fujian Medical University, Fuzhou 350122, China*
[2] *CAS Key Laboratory for Biomedical Effects of Nanomaterials and Nanosafety, CAS Center for Excellence in Nanoscience, National Center for Nanoscience and Technology, Beijing 100190, China*
[3] *School of Nanoscience and Technology, Sino-Danish College, University of Chinese Academy of Sciences, Beijing 100049, China*
[4] *Department of Laboratory Medicine, Chinese Academy of Medical Sciences & Peking Union Medical College Hospital, Beijing 100730, China*
[5] *School of Chemical Engineering and Pharmacy, Wuhan Institute of Technology, Wuhan 430205, China*
[§] *Ying Zhou, Long Wang, Lufei Chen, and Wei Wu contributed equally to this work.*

Received: 31 March 2023 / **Revised:** 10 June 2023 / **Accepted:** 12 June 2023

ABSTRACT

Glioblastoma (GBM) has been regarded as one of the most deadly and challenging cancers to treat with extremely poor prognosis. The limited efficacy of current chemotherapies might be attributed to the presence of glioma stem cells (GSCs) as well as the difficulties in passing through the blood–brain barrier (BBB) and targeting tumor cells. Tumor-derived exosomes are emerging as novel and promising drug delivery systems. However, great concerns regarding the biosafety and BBB penetrability remain to be addressed. Herein, we have developed a simple and feasible strategy to engineer GBM cell-derived exosomes with improved biosafety termed "Exo@TDPs" to deliver the cargos of chemotherapeutic agents temozolomide (TMZ) and doxorubicin (DOX) into GBM tissues. Exo@TDPs decorated with angiopep-2 (Ang-2) and CD133-targeted peptides improve the capacity to penetrate the BBB and target tumor cells. Both *in vitro* and *in vivo* studies demonstrate that Exo@TDPs can cross the BBB, target GBM cells, penetrate into deep tumor parenchyma, and release the therapeutic cargos effectively. Synergistic delivery of TMZ and DOX by Exo@TDPs exerts therapeutic effects to suppress the tumor growth and prolong the survival time of orthotopic syngeneic mouse GBM models. These findings suggest that our developed Exo@TDPs loaded with chemotherapeutic drugs may bring new possibilities for the application of tumor cell-derived exosomes for brain tumor treatment.

KEYWORDS

glioblastoma, tumor-derived exosome, peptide, temozolomide, doxorubicin, targeted chemotherapy

1 Introduction

Glioblastoma (GBM) is one of the most lethal and recalcitrant forms of human malignancies with the median survival being only 12–15 months [1–3]. Regarded as the standard of care for GBM, chemotherapy has demonstrated improved survival benefits for patients with GBM [4, 5]. As the first-line chemotherapeutic drug for GBM treatment, temozolomide (TMZ), an oral alkylating agent, has shown excellent antitumor activity, but the short half-life of averaging 1.8 h and low brain penetration (10%–20%) might limit the efficacy in both preclinical and clinical settings [6–9]. Doxorubicin (DOX) is another promising cytotoxic antitumor drug widely administered in clinical practice, and the combination of TMZ and DOX has demonstrated significantly improved clinical efficacy and has been evaluated in phase 2 clinical studies of GBM [10–12]. However, the prognosis of current GBM chemotherapies remains poor, which might be attributed to the ongoing challenges, including the presence of glioma stem cells (GSCs), poor drug blood–brain barrier (BBB) penetration contributing to inadequate concentrations in the brain, and scarce tumor targeting ability resulting in systemic toxicity [13, 14]. Thus, advanced drug delivery systems and novel therapeutic strategies are urgently needed.

With the rapid advancements in nanomedicine, artificial nano-based drug delivery systems, including liposomes, micelles, nanoparticles, and nanogels, have garnered increasing interest for cancer chemotherapy, but circulation instability, non-biodegradability, immunogenicity, and low permeability through biological membranes may hinder their further application due to unwanted side effects [15, 16]. Exosomes, naturally occurring nano-sized extracellular vesicles released from cells with a size range of 40 to 160 nm, possess unique physiochemical characteristics and have recently thrived as encouraging

Address correspondence to Xuzhen Qin, qxz_01@163.com; Zucheng Ye, zcye@uw.edu; Zhiyuan Hu, huzy@nanoctr.cn; Zihua Wang, wangzh@iccas.ac.cn

nanomaterials for delivering therapeutic agents with low toxicity, low immunogenicity, high blood stability, good biocompatibility, and satisfactory safety [17, 18]. Most importantly, recent evidence indicates that tumor-derived exosomes possess the ability to home to their parent cancer cells, offering attractive nano-drug carriers for efficient cancer chemotherapy [19, 20].

Inspired by enormous benefits achieved by engineered nanocarriers, proper modification of exosomes has emerged as a novel strategy to increase the delivery efficiency, tumor-targeting capability, and therapeutic efficacy [21]. Peptides are one of the promising candidates for targeting molecules with several potential advantages, such as higher stability, lower immunogenicity, and smaller size [22]. Angiopep-2 (Ang-2), an attractive peptide with a high affinity for low-density lipoprotein receptor-related protein 1 (LRP-1) highly expressed in both BBB endothelial cells and GBM tissues, has been recently selected for efficient BBB crossing and GBM targeting [23–25]. The CD133-positive human brain tumor cells have been regarded as cancer stem cells (CSCs) that initiate GBM, and CD133-targeted peptides are promising for the effective targeting of CSCs [26–28].

Here, we developed an effective strategy to improve the biosafety of GBM cell-derived exosomes (Exosomes) and functionalized them with peptides to enhance the BBB permeability and tumor targeting ability (Scheme 1). The engineered Exo@TDPs loaded with chemotherapeutic drugs TMZ and DOX were evaluated for the profiles of cellular uptake and drug release. *In vitro* assessment of BBB permeability and tumor cell targeting capacity of Exo@TDPs was carried out. *In vivo* and *ex vivo* biodistribution of Exo@TDPs after intravenous injection, as well as toxic side effects, were analyzed. The therapeutic effects of Exo@TDPs on GBM were determined in *in vivo* orthotopic syngeneic models. Our study offers a feasible approach for efficient cancer chemotherapy by taking advantage of peptide-engineered exosomes derived from GBM cells as promising nanocarriers reaching the brain for GBM therapy.

2 Experimental

2.1 Materials, cell lines, and animals

All chemicals, if not stated otherwise, were purchased from Sigma-Aldrich and used without any further purification, including N,N,N',N'-tetramethylethylenediamine (TMEDA), ammonium persulfate (APS), DOX, dimethyl sulfoxide (DMSO), and cell counting kit-8 (CCK-8). The transwell with permeable polyester membrane inserts was purchased from Corning. Green fluorescent protein (GFP) lentivirus and luciferase (LUC) lentivirus were purchased from GenePharma (Shanghai, China). Sulfo-cyanine 7.5 maleimide was purchased from Xi'an Qiyue Biology (Xi'an, China). TdT-mediated dUTP-biotin nick end labeling (TUNEL) assay kit was purchased from Elabscience (E-CK-A320). Specific peptides toward Ang-2 (TFFYGGSRGKRNNFKTEEYC) and CD133 (WRLRWHSPL KGGC) were screened using a high-throughput library according to previous methods [28–30]. TMZ was purchased from AbMole (Shanghai, China), frozen at −20 °C, and dissolved in DMSO into 100 mmol/mL storage solution.

Two human GBM cell lines, U251 and U87 cells, were purchased from Cell Bank of Chinese Academy of Sciences. bEnd.3 cells were purchased from Jiangsu KeyGEN BioTECH Co., Ltd. Cells were cultured in Dulbecco's Modified Eagle Medium (DMEM) (Gibco) containing 10% (*v*/*v*) fetal bovine serum (FBS) (Gibco), 100 U/mL penicillin (Gibco), and 100 μg/mL streptomycin (Gibco) at 37 °C under 5% CO_2 in a humidified incubator. Male BALB/c and BALB/c nude mice (6–10 weeks) were purchased from Charles River Laboratories (Beijing, China). All animal protocols were approved by the Institutional Animal Care and Use Committee of the National Center for Nanoscience and Technology (IACUC Issue No. NCNST21-2302-0610).

2.2 Isolation, purification, and characterizations of tumor-derived exosomes

Exosomes were purified by differential centrifugation processes, as described previously [31] with modifications. Briefly, exosome-depleted FBS was first prepared by filtering with a 100 nm filter, ultracentrifuging for 16 h, and filtering again with a 100 nm filter. When U251 GBM cells arrived at 60% confluence, the culture medium was replaced with the medium containing exosome-depleted FBS. After 72 h, the supernatant was collected and subjected to sequential centrifugation steps at 800 g for 5 min, and 2000 g for 10 min. The resulting supernatant was filtered through 0.22 μm sterilized filters (Merck Millipore) and ultracentrifuged at

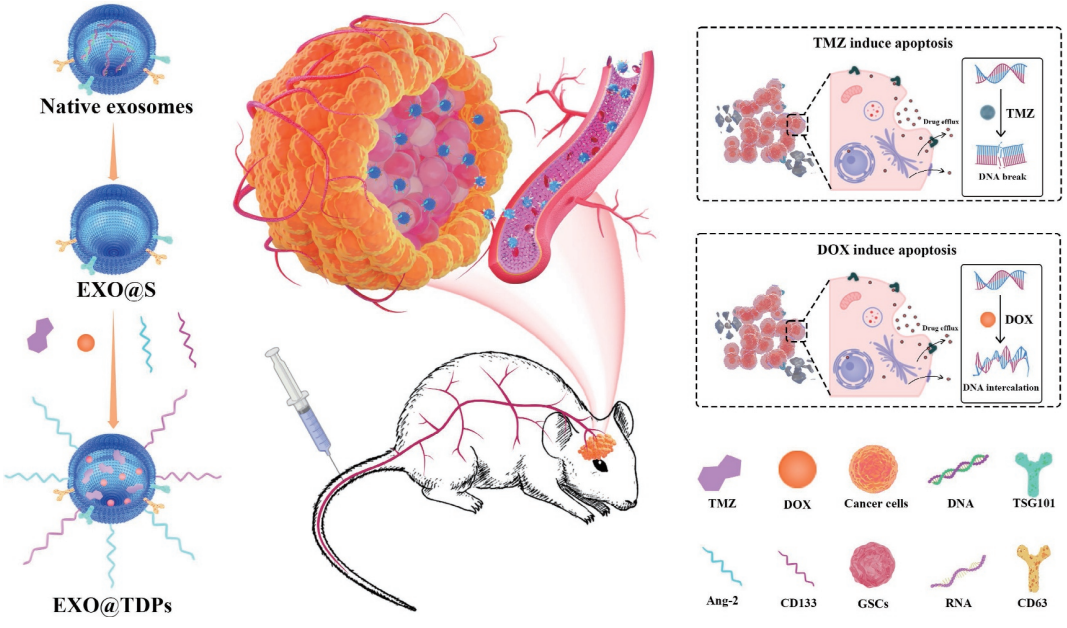

Scheme 1 Schematic illustration of the decorated Exo@TDPs with the ability to deliver the cargos of chemotherapeutic agents TMZ and DOX into GBM tissues, and exert the therapeutic effects.

100,000 g for 2 h in a SW32 Ti rotor (Beckman). Then, the pellets were resuspended in sterilized phosphate-buffered saline (PBS) followed by another 2 h of ultracentrifugation at 100,000 g. The purified exosomes were used for experimental procedures or stored at −80 °C. The morphology was observed under transmission electron microscopy (TEM). The size, zeta potential, and polydispersity index (PDI) were measured using dynamic light scattering (DLS).

2.3 Preparation of Exo@TDPs

6 mg of DSPE-PEG2000-MAL was dissolved in 0.5 mL of N,N-dimethyl formamide (DMF). 4 mg of peptides were dissolved in 2 mL of 1× PBS (pH = 7.2). The mix was slightly agitated for 48 h at 30 °C and put into a dialysis bag (cutoff molecular weight was 3500 Da). The purified exosomes were mixed with Ang-2 and CD133-targeted peptides, followed by 5 min of sonication and 2 h of incubation at 37 °C. For drug loading, the exosomes were mixed with TMZ and DOX solution at a weight ratio of 192:70:2 (*w*/*w*/*w*), followed by 6 repeated cycles of 30 s of sonication and 2 min of halt. After 1 h of incubation at 37 °C, the resulting products were successively filtered with 0.4 and 0.2 μm filters for 3 times. For fluorescent analysis of Exo@TDPs, GFP was detected at the excitation wavelength of 488 nm and the emission wavelength of 507 nm, DOX was detected at the excitation wavelength of 490 nm and the emission wavelength of 550 nm, and Cy7.5 was detected at the excitation wavelength of 788 nm and the emission wavelength of 808 nm. High-resolution fluorescence microscopic images of exosomes were observed with STELLARIS DIVE (Deep In Vivo Explorer, Leica).

2.4 Western blot analysis

Cells and harvested exosomes were lysed by radio immunoprecipitation assay (RIPA) buffer (150 mM NaCl, 0.5% ethylene diamine tetraacetic acid (EDTA), 50 mM Tris, and 0.5% NP40). Protein concentration was determined by bicinchoninic acid assay (BCA, Beyotime Biotechnology). Protein lysates were separated with sodium dodecyl sulfate-polyacrylamide gel electrophoresis (SDS-PAGE) and transferred onto polyvinylidene fluoride (PVDF) membranes. Next, the membranes were blocked with 5% non-fat milk for 2 h at room temperature, and incubated at 4 °C overnight with the indicated antibodies as follows: CD63 antibody (ab134045, 1:2000, Abcam), TSG101 antibody (ab125011, 1:1000, Abcam), and Calnexin antibody (ab133615, 1:1000, Abcam). After that, the membranes were incubated with horseradish peroxidize-conjugated secondary antibodies for 1 h at room temperature, and visualized with an ECL chemiluminescence system.

2.5 Detection of the total RNA in exosomes

Total RNA was extracted from exosomes with TRIzol Reagent (Invitrogen) and detected using SYTO® RNA Select™ Green Fluorescent Cell Stain Kit (Thermo Fisher Scientific) according to the manufacturer's instructions. The SYTO® RNA Select™ Green Fluorescent Cell Stain is a cell-permeant nucleic acid stain that is selective for RNA. Despite virtually non-fluorescent in the absence of nucleic acids, the SYTO® RNA Select™ Green Fluorescent Cell Stain could exhibit bright green fluorescence when bound to RNA and only a weak fluorescent signal when bound to DNA. The difference of total RNA levels could be detected with the excitation wavelength of 490 nm.

2.6 Release of Exo@TDPs *in vitro*

The drug release of Exo@TDPs over time was investigated at 37 °C in artificial cerebrospinal fluid (ACSF) or PBS (25 μg/mL) containing FBS. The release profiles were analyzed with high performance liquid chromatography (HPLC) (waters). Water and acetonitrile were employed as mobile phases.

2.7 BBB permeability *in vitro*

An *in vitro* BBB model was established with a tight monolayer of mouse brain endothelial bEnd.3 cells as described previously, which was considered to reasonably mimic the BBB morphology and activity [32]. Briefly, bEnd.3 cells were cultured on the transwell membrane (pore diameter of 0.4 μm) above U251, U87, or HeLa cells. When the transendothelial electrical resistance was at least 200 $\Omega \cdot cm^2$, bEnd.3 cells forming a monolayer were used for further analysis. The bottom chamber was imaged with a Leica TCS SP8 confocal microscopy.

2.8 Orthotopic syngeneic model for brain tumors

Wild-type U251 GBM cells were orthotopically inoculated into 6- to 8-week-old BALB/c mice to establish one brain tumor model. Wild-type U251 GBM cells, which were transduced with the lentivirus stably expressing luciferase, were orthotopically inoculated into 6- to 8-week-old BALB/c nude mice to establish the other brain tumor model. After anesthetization through isoflurane, mice were drilled via the skull at a position 2 mm lateral and 2 mm posterior of bregma. Cells (1×10^4 in 10 μL total volume/mouse) were stereotaxically injected at a depth of 3 mm. After 14 days, intravenously injections of 100 μL PBS, Free T/D, Exo@T/D, or Exo@TDPs into mice through the tail vein were performed every 3 days. The tumor was monitored with an *in vivo* imaging system (IVIS) (Perkin Elmer).

2.9 Immunofluorescence staining

The harvested tumors were fixed with 4% paraformaldehyde for at least 24 h, treated with gradient sucrose solution, and frozen in optimal cutting temperature (OCT) medium. Tumors were cut through a cryotome, mounted on slides, and stained with primary antibody (CD133, Abcam) overnight at 4 °C. The samples were washed in tris-buffered saline tween (TBST) for three times, followed by incubation of secondary antibodies for 1 h at room temperature. Images were obtained with fluorescence microscopy (THUNDER Imager Tissue, Leica).

2.10 Flow cytometry

The harvested tumors were homogenized to form single cell suspensions and stained with fluorescence-labeled antibodies following the manufacturer's instructions. The stained cells were detected with FACSCanto™ II (Becton Dickinson) or FACSAria III (Becton Dickinson) and analyzed using the FlowJo software (version 10.0.7, TreeStar).

2.11 Statistical analysis

All statistical analyses were carried out using GraphPad Prism 7 software. Data were presented as mean ± standard deviation (SD). Significance comparisons between groups were calculated by one-tailed unpaired *t*-test with Welch's correction. Survival analysis was performed using a log-rank test. $P < 0.05$ was considered significant if not stated otherwise.

3 Results

3.1 Manufacture and characterization of GBM cell-derived Exo@TDPs with improved biosafety

Tumor-derived exosomes have recently sparked tremendous interest as nanocarriers for chemotherapy owing to advanced characteristics including the inherent tumor cell targeting capacity

[19, 20]. To obtain a pool of high-purity tumor-derived exosomes for GBM treatment, we isolated and purified the naturally-equipped exosomes (Exosomes) from the cultured medium of human U251 GBM cells by differential ultracentrifugation processes as described previously [31] with modifications. The harvested Exosomes exhibited a typical membrane-bound and cup-shaped morphology characterized by TEM observation (Fig. 1(a) and Fig. S1 in the Electronic Supplementary Material (ESM)). Western blot experiments further indicated that the obtained Exosomes were positive for exosome-specific markers cluster of differentiation 63 (CD63) and tumor susceptibility gene 101 (TSG101) (Fig. 1(b) and Fig. S2 in the ESM). By contrast, the non-exosome marker calnexin, a membrane-bound protein located in the endoplasmic reticulum (ER), was only observed in the group of whole cell lysates, demonstrating the high purity of isolated exosomes.

Although tumor-derived exosomes have exhibited unique advantages, the potential protumoral risks of their original cargos might lead to safety concerns, and innovative approaches are warranted to solve this issue. To diminish the risks of GBM cell-derived exosomes, we developed a sonication-mediated cargo elimination method with improved biosafety. Compared with the controlled Exosomes group, the group with the treatment of sonication (Exo@S) demonstrated a dominant decline of protein contents, as visualized by Coomassie brilliant blue (CBB) staining using SDS-PAGE (Figs. 1(c) and 1(d)). Apart from proteins, RNAs as the other predominant component of exosomes were also found to be decreased by sonication treatment. The data of RNA quantification showed that a large amount of RNAs were eliminated after sonication (Fig. 1(d)). The mRNAs associated with cell proliferation (IDH1), angiogenesis (VGER), invasion (EGFR), and migration (TGFB1) [33–35] were selected for RNA eliminating efficiency analysis, and the primers are listed in Table S1 in the ESM. The results of real-time quantitative polymerase chain reaction (RT-qPCR) suggested that these protumoral RNA molecules were reduced after sonication treatment (Fig. 1(e)). Furthermore, the elimination of the original cargos through sonication showed obvious proliferation inhibition effects to diminish the protumoral functions of tumor-derived exosomes (Fig. S3 in the ESM). The data of wound healing assays also indicated that the effects of the Exosomes group on tumor migration were not observed in the Exo@S group, suggesting a decline of protumoral cargos after sonication (Fig. S4 in the ESM). These results confirmed the effectiveness of sonication-mediated cargo elimination strategy, which preserved the main physical properties of tumor-derived exosomes with improved biosafety.

To further explore the potential therapeutic roles of Exo@S in GBM treatment, we engineered the exosome-sheathed nanocarriers Exo@TDPs by loading TMZ and DOX into the exosomes as well as functionalizing the exosomes with Ang-2 and CD133-targeted peptides according to the previous methods [28–30]. The targeting abilities of Ang-2 and CD133-targeted peptides have been verified [36, 37], and their mass spectrometry data are shown in Fig. S5 in the ESM. After drug loading and surface modification with targeted peptides, the slightly hollow shape seemed to be plump, suggesting a tendency to be filled.

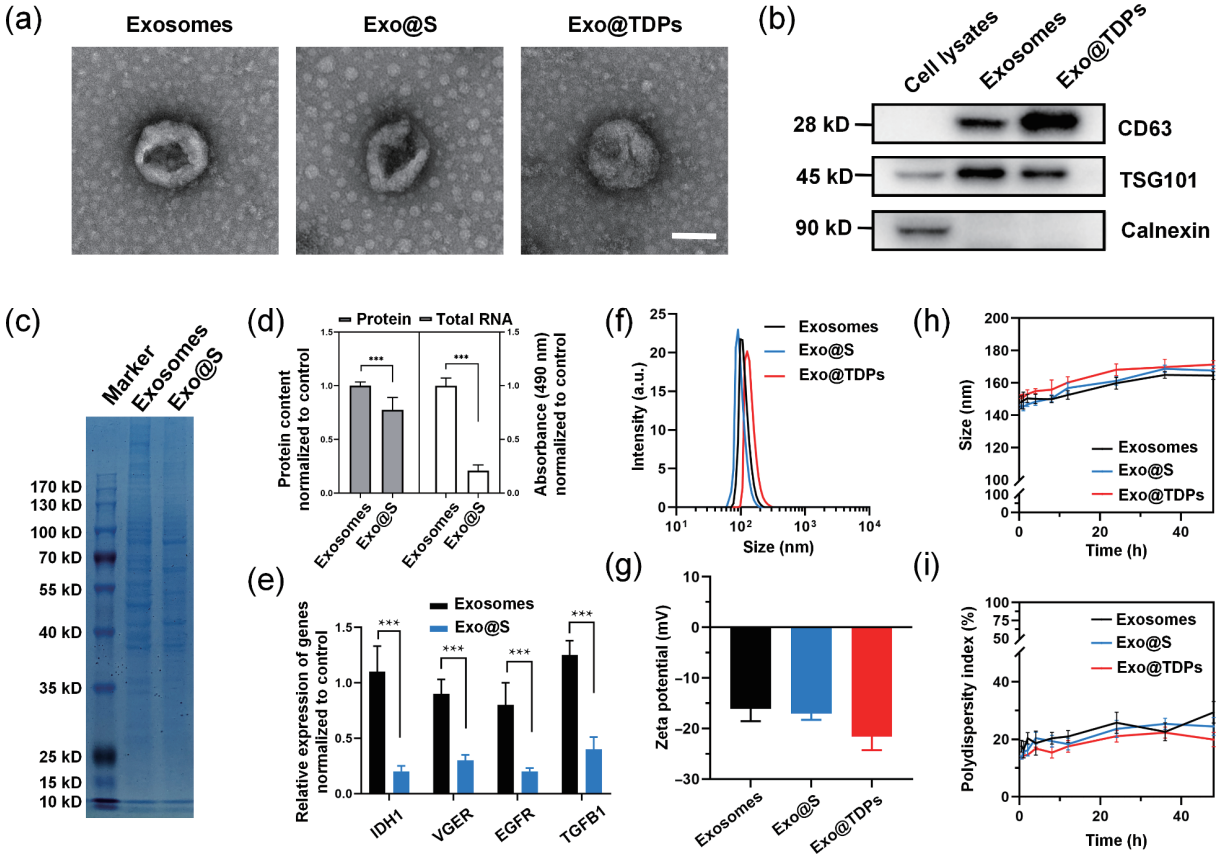

Figure 1 Evaluation of engineered sonication-mediated GBM cell-derived exosomes with elimination of the original cargos. (a) TEM images of the controlled Exosomes group, the Exo@S group, and the TMZ/DOX-loaded as well as Ang-2/CD133-targeted peptides-engineered (Exo@TDPs) group. Scale bar, 100 nm. (b) Immunoblotting analysis of exosome-specific markers (CD63 and TSG101) and a non-exosome marker (Calnexin). (c) CBB staining of the proteins between Exosomes and Exo@S groups in SDS-PAGE. (d) The total proteins analyzed by BCA assay and the total RNAs detected using SYTO RNA select dye between Exosomes and Exo@S groups. (e) RT-qPCR analysis of the mRNA expression of IDH1, VGER, EGFR, and TGFB1 between Exosomes and Exo@S groups. (f) Hydrodynamic diameter of Exosomes, Exo@S, and Exo@TDPs groups by DLS analysis. (g) Zeta-potential of Exosomes, Exo@S, and Exo@TDPs groups. (h) Size distribution of Exosomes, Exo@S, and Exo@TDPs groups within 48 h. (i) Change of PDI in Exosomes, Exo@S, and Exo@TDPs groups within 48 h. Data were presented as mean ± SD ($n = 3$). ***$P < 0.001$.

Nevertheless, the morphology and size of Exo@S group and Exo@TDPs group were not obviously altered compared with Exosomes group (Fig. 1(a)). As shown in a larger field of view, the morphology and size among the three groups remained similar analyzed by TEM observation (Fig. S1 in the ESM), indicating that the treatments including sonication did not cause obvious damage to the structure of exosomes. Moreover, relative quantification of the protein expression levels between the Exo@TDPs group and Exosomes group showed that their exosome membrane proteins were not statistically different (Fig. S2(d) in the ESM), suggesting that the number of exosomes was not obviously decreased after sonication and filtration. The individual drug efficacy of TMZ or DOX was investigated, and the optimal dosage ratio of the two drugs was confirmed priorly (Fig. S6 in the ESM). The hydrodynamic diameter of Exo@TDPs was 151.9 nm measured by DLS analysis, whereas sonication treatment, drug loading, and surface modification did not dramatically alter the size of tumor-derived exosomes (Fig. 1(f)). The zeta-potential of Exo@TDPs and other groups was all negative (Fig. 1(g)). Among three groups, there were no significant changes in particle size (Fig. 1(h)) and PDI (Fig. 1(i)) within 48 h. Collectively, the above data indicate that the sonication-mediated and engineered Exo@TDPs derived from GBM cells can be used as novel exosome-sheathed nanocarriers for chemotherapy.

3.2 High-resolution live-cell imaging of Exo@TDPs with assessment of cellular uptake, drug release, and CD133 colocalization

To confer the purposes of cell imaging and drug delivery tracking, we took advantage of a near-infrared (NIR) dye cyanine 7.5 (Cy7.5) for direct visualization under fluorescent microscope. In a genetically engineered U251 GBM cell line stably expressing GFP, cells were labeled with Cy7.5, and the corresponding GFP- and Cy7.5-labeled Exo@TDPs were obtained. High-resolution fluorescence microscopic images clearly confirmed the colocalization of DOX (an aggregation caused quenching fluorescence compound with red emission) [38] and exosomes isolated from GFP- and Cy7.5-labeled U251 GBM cells, demonstrating the successful encapsulation of drugs into Exo@TDPs (Fig. 2(a) and Fig. S7 in the ESM). Notably, we successfully snapped the images of Exo@TDPs with extremely high resolution, and the Cy7.5-labeled exosomes remained functional under a confocal laser scanning microscopy without

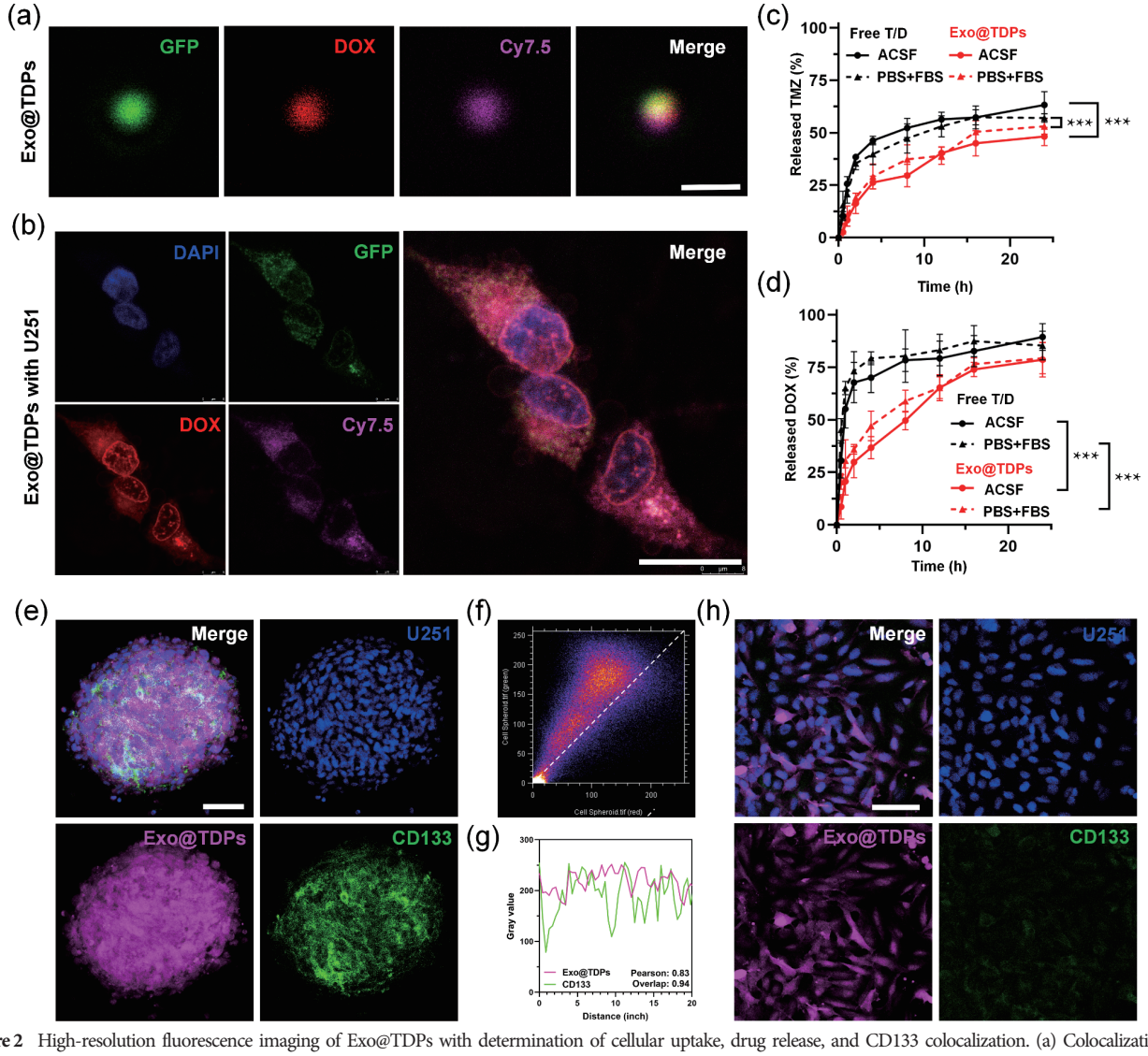

Figure 2 High-resolution fluorescence imaging of Exo@TDPs with determination of cellular uptake, drug release, and CD133 colocalization. (a) Colocalization of DOX and exosomes isolated from GFP- and Cy7.5-labeled U251 GBM cells by confocal microscopy. Scale bar, 200 nm. (b) Live-cell imaging of GFP- and Cy7.5-labeled Exo@TDPs targeting and taken up by wild-type U251 GBM cells. Scale bar, 20 μm. (c) Cumulative release profiles of TMZ from Exo@TDPs group or Free T/D group dispersed in ACSF or PBS containing FBS. (d) Cumulative release profiles of DOX from Exo@TDPs group or Free T/D group dispersed in ACSF or PBS containing FBS. (e) Fluorescence images of the tumor sphere formed by U251 GBM cells. Scale bar, 50 μm. (f) Fluorescence analysis of the cell spheroid. (g) Gray value of fluorescence images. (h) Fluorescence images of U251 GBM cells. Data were presented as mean ± SD ($n = 3$). ***$P < 0.001$.

fixation of cells, offering an innovative strategy to observe the exosomes and trace the targeting effects.

To visualize the cellular uptake of exosomes, we incubated the above-mentioned GFP- and Cy7.5-labeled Exo@TDPs with wild-type U251 GBM cells. High-resolution live-cell imaging systems could be applied to monitor the internalization process of Exo@TDPs. As depicted in Fig. 2(b), the fluorescent signals of Exo@TDPs were dispersed within the cytoplasm, indicating that the exosomes were efficiently internalized and taken up by U251 GBM cells. DOX was observed to distribute throughout the cytoplasm and nuclei, suggesting an effective drug accumulation in tumor cell nuclei which could enhance anticancer potency. Moreover, the drug release behavior of Exo@TDPs over time was assessed in both ACSF and PBS containing FBS, which imitated the *in vivo* environment of brain and blood, respectively. Compared with the free TMZ or DOX group, Exo@TDPs showed a sustained drug release profile in which both TMZ (Fig. 2(c)) and DOX (Fig. 2(d)) were gradually released, demonstrating that the chemotherapeutic agents might be well protected by the Exo@TDPs which could avoid undesirable drug burst release in blood circulation. In addition, the targeting ability of Exo@TDPs on GSCs was verified using tumor sphere formation assays. The tumor sphere formed by U251 GBM cells could present strong expression of CD133 (Fig. 2(e)). Colocalization of Exo@TDPs and CD133 was observed in the cell spheroid (Figs. 2(f) and 2(g)). By contrast, the signals of CD133 were very weak in U251 GBM cells without the formation of tumor sphere (Fig. 2(h)). Overall, these observations confirm that Exo@TDPs are internalized by GBM cells, release the cargos of TMZ as well as DOX effectively, and target CD133-positive GSCs.

3.3 *In vitro* evaluation of BBB permeability and target-homing capability of Exo@TDPs

The biological barrier crossing and intrinsic targeting properties of nanocarriers are vital for high transportation of chemotherapeutic drugs to tumor sites in the brain [13, 14, 39]. Therefore, an *in vitro* model for the BBB penetration was employed to assess the ability to cross the BBB-mimicking cell monolayer. The Exo@S isolated from GFP- and Cy7.5-labeled U251 GBM cells was incubated with a tight monolayer of bEnd.3 cells cultured on the insert of the transwell (Fig. 3(a)). Different types of tumor cells including U251, U87, and HeLa cells were grown in the bottom chamber. The results indicated that the fluorescence signals in U251 GBM cell group were the highest (Fig. 3(b)) by analyzing the green fluorescence images (Fig. S8 in the ESM) in the bottom chamber, demonstrating the superior self-targeting homing ability of U251-derived Exo@S to the homologous tumor with excellent BBB penetration and biocompatibility properties. The preferential uptake of U251-derived Exo@S by U251 GBM cells suggested the

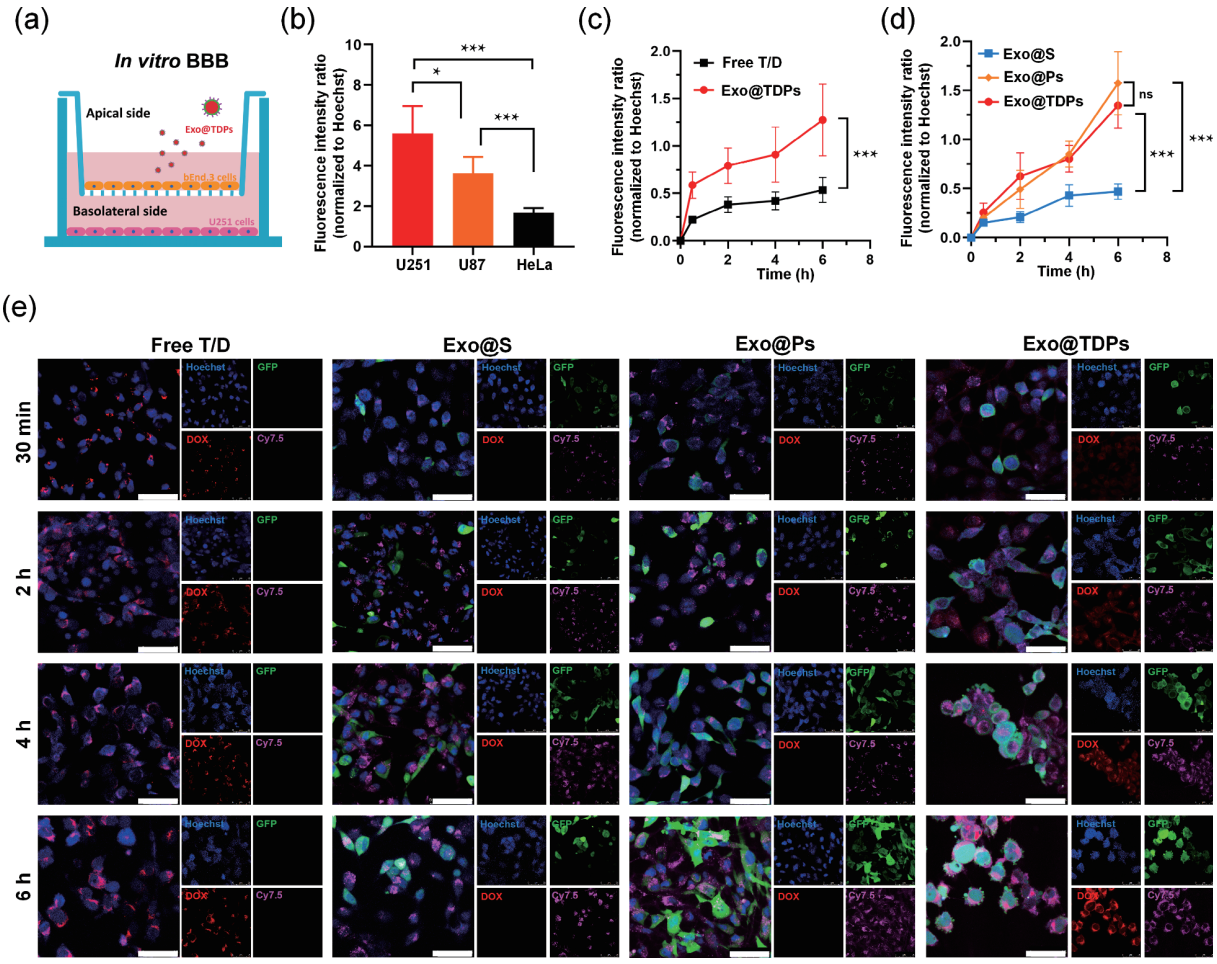

Figure 3 *In vitro* assessment of BBB penetration and homotypic targeting ability of Exo@TDPs. (a) Schematic of the *in vitro* BBB model. (b) The GFP fluorescence intensity ratio of wild-type U251, U87, or HeLa cells in the basolateral side with a tight monolayer of bEnd.3 cells cultured on the insert of the transwell treated with the Exo@S isolated from GFP- and Cy7.5-labeled U251 GBM cells. (c) The red fluorescence intensity ratio of wild-type U251 GBM cells in the basolateral side with bEnd.3 cells cultured on the transwell insert treated with the Free T/D and Exo@TDPs isolated from GFP- and Cy7.5-labeled U251 GBM cells. (d) The GFP fluorescence intensity ratio of wild-type U251 GBM cells in the basolateral side with bEnd.3 cells cultured on the transwell insert treated with the Exo@S, Ang-2/CD133-targeted peptides-engineered exosomes (Exo@Ps), and Exo@TDPs isolated from GFP- and Cy7.5-labeled U251 GBM cells. (e) Fluorescence images of wild-type U251 GBM cells in the basolateral side with bEnd.3 cells cultured on the transwell insert treated with Free T/D, Exo@S, Exo@Ps, or Exo@TDPs isolated from GFP- and Cy7.5-labeled U251 GBM cells at 30 min, 2 h, 4 h, and 6 h. Data were presented as mean ± SD ($n = 3$). *$P < 0.05$; ***$P < 0.001$; ns, not significant.

cell-type tropism for tumor-derived exosomes. Moreover, the drug release profile was determined with wild-type U251 cells cultured in the bottom chamber by detecting the red fluorescence of DOX. Compared with the Free T/D group, Exo@TDPs significantly enhanced the drug delivery crossing the BBB and uptake efficiency into U251 GBM cells (Fig. 3(c)). Furthermore, Exo@S group, Ang-2/CD133-targeted peptides-engineered exosome (Exo@Ps) group, and Exo@TDPs group harvested from GFP- and Cy7.5-labeled U251 GBM cells were compared. The observations confirmed that Ang-2 and CD133-targeted peptides dramatically improved the ability to penetrate the BBB and deliver drugs into U251 cells by measuring the fluorescence imaging of GFP (Fig. 3(d)) and Cy7.5 (Fig. S9 in the ESM). The fluorescence images of U251 cells in the bottom chamber treated with Free T/D, Exo@S, Exo@Ps, or Exo@TDPs at various time points are exhibited in Fig. 3(e). Compared with the Free T/D group which was negative for GFP and Cy7.5 due to the absence of the exosomes, the fluorescence signals of the Exo@S, Exo@Ps, and Exo@TDPs groups were gradually accumulated in a time-dependent manner. In contrast to the Free T/D group, the Exo@TDPs group demonstrated a significant increase in DOX delivery efficiency crossing the endothelial cell barrier. Notably, some morphologic features of apoptosis were found in U251 GBM cells after 4 h of Exo@TDPs treatment, suggesting the therapeutic roles of the engineered exosomes. All the above findings imply that Exo@TDPs enhance the BBB permeability of chemotherapeutic agents and home to the parent cancer cells to exert the antitumor effects.

3.4 *In vivo* and *ex vivo* biodistribution of Exo@TDPs and toxicity evaluation

In order to examine the biodistribution of Exo@TDPs in orthotopic syngeneic models, GFP- and Cy7.5-labeled Exo@TDPs or Exo@S as control were intravenously injected into the BALB/c mice bearing wild-type U251 GBM tumors in the brain, and fluorescent images were obtained using an IVIS fluorescence imaging device. The tumors in the extracted brain tissues exhibited strong green fluorescence signals at 24 h after injection, demonstrating excellent tumor targeting ability of Exo@TDPs towards GBM tumors (Fig. 4(a)). However, when the alive mice were imaged directly without brain extraction, the GFP signals were found incompetent to show the true positive results, probably caused by the existence of hair. Therefore, to solve this issue, Cy7.5 was used for fluorescence imaging analysis. Compared with the control group, stronger signals of Cy7.5 in the

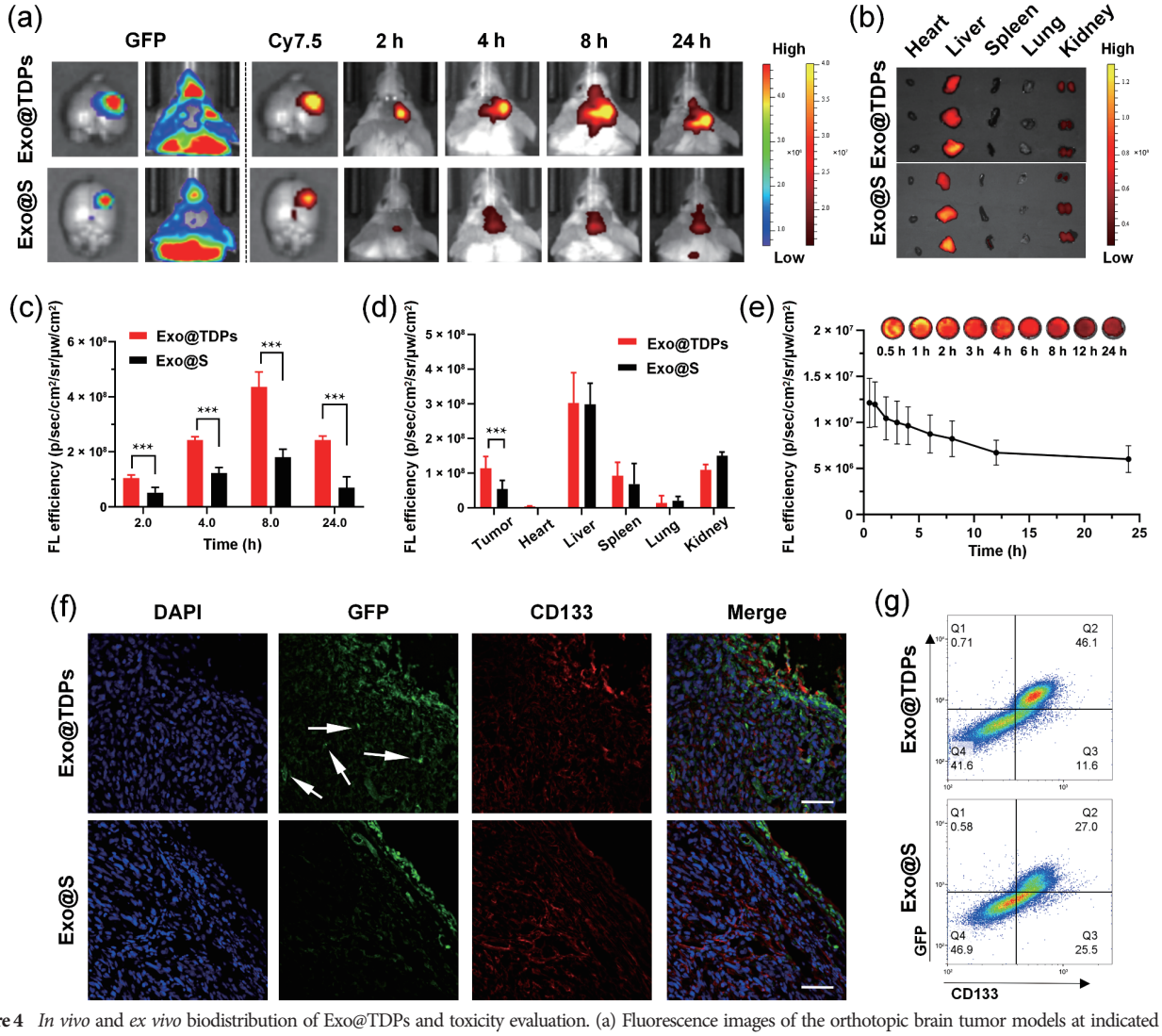

Figure 4 *In vivo* and *ex vivo* biodistribution of Exo@TDPs and toxicity evaluation. (a) Fluorescence images of the orthotopic brain tumor models at indicated time points after intravenously injected with GFP- and Cy7.5-labeled Exo@TDPs or Exo@S. (b) *Ex vivo* fluorescence imaging of heart, liver, spleen, lung, and kidney harvested from mice treated with Exo@TDPs or Exo@S. (c) Quantitative analysis of *ex vivo* fluorescence efficiency of Exo@TDPs and Exo@S groups in the brain at indicated time points after intravenously injection. (d) Quantitative analysis of *ex vivo* fluorescence efficiency of Exo@TDPs and Exo@S groups in the tumors and the main organs including heart, liver, spleen, lung, and kidney. (e) Quantitative analysis of the fluorescence signals at different time points in the blood of mice after injection of Exo@TDPs. (f) Fluorescence images of Exo@TDPs and Exo@S groups penetrating into the tumor parenchyma. Scale bar, 100 μm. (g) Representative flow cytometric analysis images of the dissected tumors in Exo@TDPs and Exo@S groups. Data were presented as mean ± SD ($n = 3$). ***$P < 0.001$.

Exo@TDPs group demonstrated the increased targeted delivery of Exo@TDPs to GBM tumors in the brain in a time-dependent manner.

To further evaluate the toxic side effects of Exo@TDPs in the body, the main organs including heart, liver, spleen, lung, and kidney were harvested and analyzed. Fluorescent signals were observed mainly in the liver and kidney but not in other organs (Fig. 4(b)). Quantitative analysis indicated that the fluorescence efficiency of Exo@TDPs was higher compared with that of Exo@S in the brain (Fig. 4(c)) rather than in the main organs (Fig. 4(d)), demonstrating that Ang-2 and CD133-targeted peptides greatly enhanced the BBB penetration. In addition, hematoxylin and eosin (H&E) staining of histological section from the main organs indicated that apparent histopathological abnormalities or lesions were not observed (Fig. S10 in the ESM). In the blood of mice after intravenous injection, the fluorescence signals were gradually decreased over time (Fig. 4(e)).

CD133, a GSC marker, was found to be a valuable predictor for the survival probability of patients with gliomas (Fig. S11 in the ESM) based on the Chinese Glioma Genome Atlas (CGGA) [40]. Immunofluorescence staining of CD133 was then conducted to analyze the colocalization of Exo@TDPs and GBM tumors. Notably, Exo@TDPs showed enhanced penetration into deep tumor parenchyma to target CD133-positive GBM cells (Fig. 4(f)). The number of colocalization between Exo@TDPs and CD133 was elevated compared with the Exo@S group (Fig. S12 in the ESM), suggesting the advantages of Exo@TDPs in targeting GSCs. Flow cytometry analysis of the dissected tumors further demonstrated that Exo@TDPs increased the double positive signals (green and red) (Fig. 4(g)). The Exo@TDPs with CD133-targeted peptides had stronger colocalization effects compared with Exo@S (46.1% ± 1.2% vs. 27.0% ± 0.7%, $P < 0.001$, $n = 3$), suggesting the superior targeting ability on GSCs *in vivo*. Taken together, these data show that Exo@TDPs transport through the BBB effectively and improve the targeting effects on GBM tumors as well as deep penetration ability without significant toxicity to the main organs, revealing the well-tolerated biosafety.

3.5 Exo@TDPs-mediated therapeutic effects in *in vivo* orthotopic syngeneic models for GBM

To explore the potential therapeutic effects of Exo@TDPs, we established orthotopic syngeneic models of BALB/c nude mice bearing luciferase-labeled U251 GBM tumors in the brain (Fig. 5(a)). Free drug group was also compared with evaluate the potential advantages of Exo@TDPs. Intravenously injections of PBS, Free T/D, Exo@T/D which lacked Ang-2/CD133-targeted peptides, and Exo@TDPs into mice through the tail vein every 3 days since day 14 were carried out to determine whether Exo@TDPs facilitated drug delivery across the BBB and targeted GBM with effective chemotherapy *in vivo*. In the PBS control group, the GBM tumor grew gradually in a time-dependent manner assessed by bioluminescence imaging, which was only observed restrictedly in the brain (Fig. 5(b)). At day 56 after intravenous injections, the fluorescence intensity in the Exo@TDPs group was significantly reduced compared with that in the Exo@T/D group (Fig. 5(c)), suggesting inhibited growth of GBM tumors. The injections did not obviously alter the body weight of mice in all groups (Fig. S13 in the ESM). Contrasted with other groups, the survival time of the mice treated with Exo@TDPs was longer, demonstrating an improved survival benefit (Fig. 5(d)). The extracted brain tissues were sectioned for histological analysis, and the representative images revealed that Exo@TDPs exhibited an obviously increased efficacy in tumor inhibition compared with other groups (Fig. 5(e), upper panels). Similar results were found in the TUNEL assay, as the green signals were significantly elevated in the Exo@TDPs group (Fig. 5(e), lower panels). The dramatically enhanced cytotoxic antitumor activity (Fig. 5(f)) might be explained by the higher concentrations of drugs in the orthotopic GBM region, which could be visualized by fluorescent DOX (Fig. 5(g)). In summary, the results suggest that Exo@TDPs efficiently transport through the BBB and deliver the chemotherapeutic agents to the tumor region in the brain to achieve GBM suppression.

4 Discussion

Although rapidly accumulating evidence implicates that exosomes, specifically tumor-derived exosomes, have emerged as a promising nanoscale drug delivery platform exhibiting tumor-preferential accumulation, great concerns including the biosafety in application and BBB penetration ability remain to be solved. In the present study, the sonication-mediated Exo@TDPs derived from GBM cells were demonstrated to be effective exosome-sheathed nanocarriers with improved biosafety. The engineered Exo@TDPs loaded with chemotherapeutic drugs TMZ and DOX could be uptaken by GBM cells and release the cargos effectively. Moreover, Exo@TDPs presented high BBB permeability and good homotypic targeting ability *in vitro*. Furthermore, targeted delivery of drugs by Exo@TDPs to GBM tumors was observed to be effective without visible toxicity to the main organs *in vivo*. In orthotopic syngeneic models, Exo@TDPs exerted therapeutic effects to inhibit the growth of GBM tumors and prolonged the survival time of GBM-bearing mice.

In recent years, tumor-derived exosomes have been demonstrated to be effective and safe nanocarriers for targeted therapy applications [19, 20, 41]. However, how to diminish their potential protumoral functions remains a challenging issue. The effects of exosomes on cancer progression are presumed to be determined by the cargos [42]. Thus, to overcome the limitation, we explored an effective strategy by combining the traditional differential ultracentrifugation with sonication. We discovered that sonication-mediated cargo elimination method improved the biosafety of tumor-derived exosomes without affecting the main physical properties. Consistent with our strategy, saponin treatment was also found to achieve the leakage of the cargo molecules by increasing the membrane permeability of exosomes [43]. The improvement of biosafety through various approaches may herald a broader clinical application of tumor-derived exosomes as nanocarriers for chemotherapy.

The existence of BBB is considered to restrict the transport of TMZ and DOX from reaching the brain [44]. The lack of targeting ability further leads to inadequate concentrations in the tumor site as well as systemic toxicities [14]. Nanocarriers, however, provide viable tools for synergistic combinations of different chemotherapeutic drugs with improved safety and efficacy [45]. Accordingly, we functionalized the tumor-derived exosomes with the BBB crossing peptide Ang-2 and the peptide targeting CD133-presenting CSCs [23–28]. Our observations revealed the engineered Exo@TDPs exhibited the BBB penetration and cancer targeting abilities both *in vitro* and *in vivo*. Consistently, angiopep-2 peptide and anti-CD133 monoclonal antibody were also conjugated to a liposome for BBB transcytosis and specific delivery to GBM stem cells, which are known to exert the drug resistance [46]. Multi-functional nanocarriers may offer potential avenues for GBM chemotherapy by surmounting current therapeutic challenges including poor BBB penetration and weak infiltration into tumors.

In spite of our incomplete understanding of the biology of tumor-derived exosomes, their unique characteristics of tumor-targeting property have been exploited [19, 20]. The exosomes

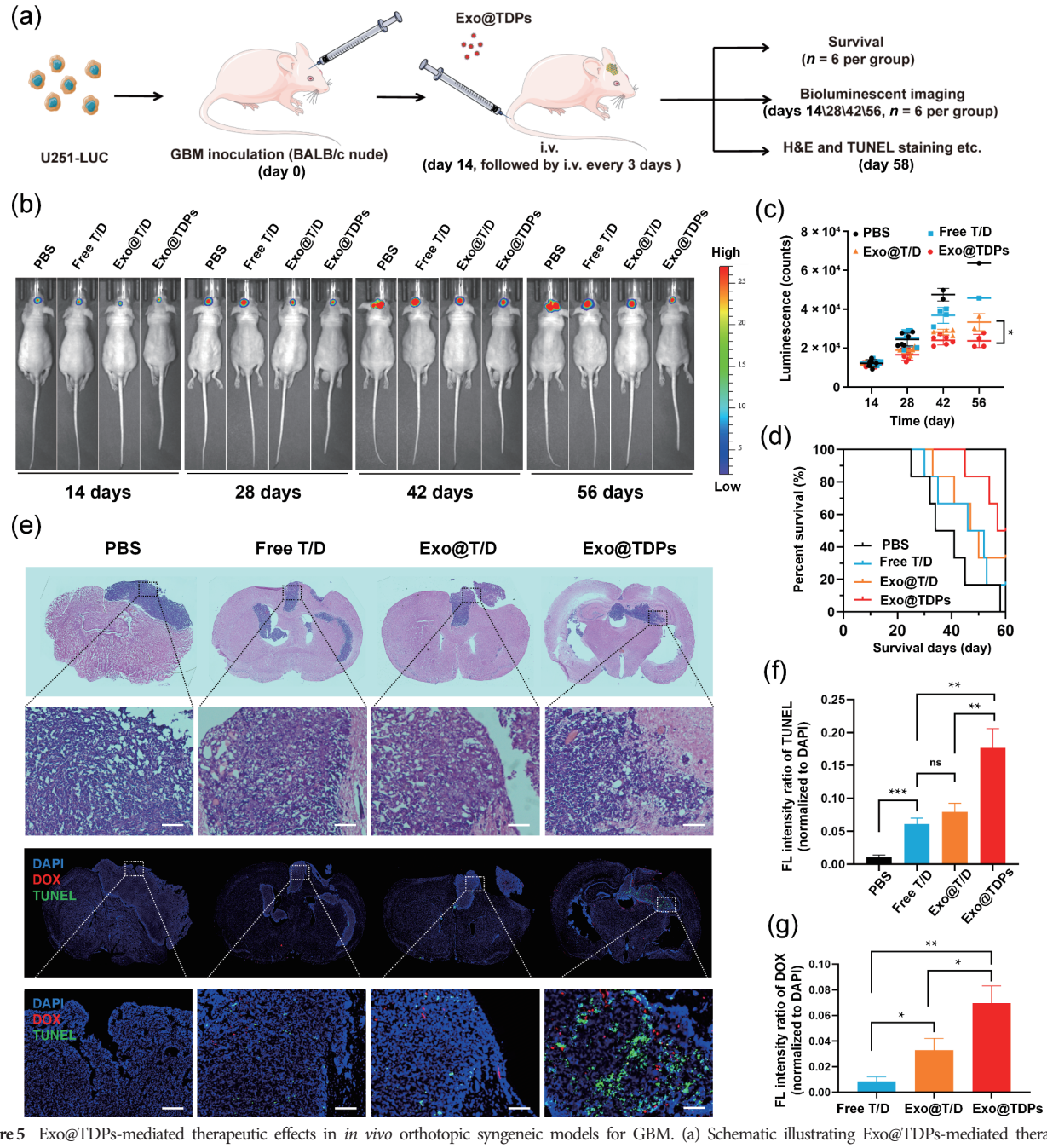

Figure 5 Exo@TDPs-mediated therapeutic effects in *in vivo* orthotopic syngeneic models for GBM. (a) Schematic illustrating Exo@TDPs-mediated therapy in orthotopic syngeneic models of BALB/c nude mice bearing luciferase-labeled U251 GBM tumors in the brain. (b) Imaging of *in vivo* bioluminescence of BALB/c nude mice bearing luciferase-labeled U251 GBM tumors in the brain in response to treatment with PBS, Free T/D, Exo@T/D, and Exo@TDPs at days 14, 28, 42, and 56 after intravenously injections through the tail vein. (c) Bioluminescence intensity of luciferase-labeled U251 GBM-bearing mice treated with PBS, Free T/D, Exo@T/D, and Exo@TDPs at days 14, 28, 42, and 56, respectively. (d) Kaplan–Meier survival curves of mice in different groups. (e) Histochemical analysis of the extracted brain sections in different groups subjected to H&E staining (upper panels) and immunofluorescence analysis of the extracted brain sections in different groups analyzed by TUNEL assay (green) and visualized by fluorescent DOX (red) (lower panels). Scale bar, 200 μm. (f) Quantitative analysis of fluorescence intensity ratio of TUNEL assay results in different groups. (g) Quantitative analysis of fluorescence intensity ratio of DOX evaluation in different groups. Data were presented as mean ± SD ($n = 3$). $^*P < 0.05$; $^{**}P < 0.01$; $^{***}P < 0.001$; ns, not significant.

derived from tumor cells might exert biocompatible and efficient tumor targeting abilities towards their parent cancer cells due to the inherent homotypic adhesion properties [47, 48]. The human GBM cell line U251-derived exosomes showed superior targeting ability compared with the group of human cervical cancer HeLa cells, suggesting the superior self-targeting homing ability of U251-derived exosomes to the homologous tumor with excellent biological barrier crossing ability during the brain targeting delivery. Interestingly, U251 and U87 were both human GBM cell lines, but the exosomes derived from U251 GBM cells demonstrated the preferential uptake by their parent cancer cells rather than U87 GBM cells. The findings suggested that patient plasma-derived exosomes and other sources of exosomes might serve as chemotherapy drug carriers to exert potential therapeutic effects in the clinical settings. Despite the intrinsic abilities, decorating or incorporating materials with exosomes is also needed to present superior properties, such as increasing the lesion accumulation in the tumor site within the brain [49]. Interestingly, tumor-derived exosomes also demonstrate diagnostic and prognostic values as promising biomarkers for glioma [50]. Further investigations are necessary to explore the potential clinical application of tumor-derived exosomes.

A broad spectrum of membrane proteins on the surface of exosomes might determine their adhesion and targeting

capabilities [51]. Our data indicated that the structure and shape of exosomes did not show obvious differences with the treatment of sonication, whereas the size of exosomes tended to decrease slightly after sonication, suggesting that this cargo elimination strategy might result in reducing the inner cargos rather than the membrane proteins. Nevertheless, whether sonication influences the membrane proteins of tumor-derived exosomes as well as their abilities remains to be further explored with more in-depth investigation in future research. In addition, CD133 expression has been found to be correlated with glioma grade [52]. Therefore, if more validated biomarkers for different grades of glioma can be used for targeted tumor therapy, the therapeutic effects of drug-loaded nanocarriers might be beneficial in a relatively early period.

5 Conclusions

In conclusion, we have successfully developed an effective strategy to engineer GBM cell-derived exosomes as biosafe nanocarriers for GBM targeted chemotherapy. The decorated Exo@TDPs effectively transport through the BBB, target GBM cells, penetrate into deep tumor parenchyma, and release the cargos. Following intravenous injection, Exo@TDPs demonstrate enhanced tumor targeting ability and improved therapeutic effects. Our results suggest that the engineered Exo@TDPs derived from GBM cells with improved biosafety have the clinical potential as drug nanocarriers for efficient targeted chemotherapy of GBM.

Acknowledgements

The authors would like to thank the facilities and technical assistance of the Public Technology Service Center (Fujian Medical University, Fuzhou, China). This work was financially supported by the National Natural Science Foundation of China (Nos. 32027801, 81801766, and 31870992), the Strategic Priority Research Program of Chinese Academy of Sciences (Nos. XDB36000000 and XDB38010400), Science and Technology Service Network Initiative of the Chinese Academy of Sciences (No. KFJ-STS-ZDTP-079), CAS-JSPS (No. GJHZ2094), National High-Level Hospital Clinical Research Funding (No. 2022-PUMCH-A-059), Fujian Medical University Foundation for the Introduction of Talents (Nos. XRCZX2019018, XRCZX2017020, and XRCZX2019005), the Joint Funds for the innovation of science and Technology Fujian Province (No. 2019Y9001), the Natural Science Foundation of Fujian Province (Nos. 2020J01599, 2022J01203, and 2022J01666), and the Natural Science Foundation of Tibet Autonomous Region (No. XZ2021ZR-ZY13(Z)).

Electronic Supplementary Material: Supplementary material (further details of TEM images with a larger field of view, immunoblotting analysis, cell proliferation, cell migration, mass spectrometry data of the peptides, drug efficacy, fluorescence images, histochemical analysis, and weight changes of mice) is available in the online version of this article at https://doi.org/10.1007/s12274-023-5921-6.

References

[1] Wen, P. Y.; Kesari, S. Malignant gliomas in adults. *N. Engl. J. Med.* **2008**, *359*, 492–507.

[2] Alexander, B. M.; Cloughesy, T. F. Adult glioblastoma. *J. Clin. Oncol.* **2017**, *35*, 2402–2409.

[3] Lapointe, S.; Perry, A.; Butowski, N. A. Primary brain tumours in adults. *Lancet* **2018**, *392*, 432–446.

[4] Stupp, R.; Mason, W. P.; van den Bent, M. J.; Weller, M.; Fisher, B.; Taphoorn, M. J. B.; Belanger, K.; Brandes, A. A.; Marosi, C.; Bogdahn, U. et al. Radiotherapy plus concomitant and adjuvant temozolomide for glioblastoma. *N. Engl. J. Med.* **2005**, *352*, 987–996.

[5] Stupp, R.; Hegi, M. E.; Mason, W. P.; van den Bent, M. J.; Taphoorn, M. J. B.; Janzer, R. C.; Ludwin, S. K.; Allgeier, A.; Fisher, B.; Belanger, K. et al. Effects of radiotherapy with concomitant and adjuvant temozolomide versus radiotherapy alone on survival in glioblastoma in a randomised phase III study: 5-year analysis of the EORTC-NCIC trial. *Lancet Oncol.* **2009**, *10*, 459–466.

[6] Hammond, L. A.; Eckardt, J. R.; Baker, S. D.; Eckhardt, S. G.; Dugan, M.; Forral, K.; Reidenberg, P.; Statkevich, P.; Weiss, G. R.; Rinaldi, D. A. et al. Phase I and pharmacokinetic study of temozolomide on a daily-for-5-days schedule in patients with advanced solid malignancies. *J. Clin. Oncol.* **1999**, *17*, 2604.

[7] Ostermann, S.; Csajka, C.; Buclin, T.; Leyvraz, S.; Lejeune, F.; Decosterd, L. A.; Stupp, R. Plasma and cerebrospinal fluid population pharmacokinetics of temozolomide in malignant glioma patients. *Clin. Cancer Res.* **2004**, *10*, 3728–3736.

[8] Portnow, J.; Badie, B.; Chen, M. K.; Liu, A.; Blanchard, S.; Synold, T. W. The neuropharmacokinetics of temozolomide in patients with resectable brain tumors: Potential implications for the current approach to chemoradiation. *Clin. Cancer Res.* **2009**, *15*, 7092–7098.

[9] Jatyan, R.; Singh, P.; Sahel, D. K.; Karthik, Y. G.; Mittal, A.; Chitkara, D. Polymeric and small molecule-conjugates of temozolomide as improved therapeutic agents for glioblastoma multiforme. *J. Control. Release* **2022**, *350*, 494–513.

[10] Chua, S. L.; Rosenthal, M. A.; Wong, S. S.; Ashley, D. M.; Woods, A. M.; Dowling, A.; Cher, L. M. Phase 2 study of temozolomide and Caelyx in patients with recurrent glioblastoma multiforme. *Neuro-Oncol.* **2004**, *6*, 38–43.

[11] Ananda, S.; Nowak, A. K.; Cher, L.; Dowling, A.; Brown, C.; Simes, J.; Rosenthal, M. A.; Cooperative Trials Group for Neuro-Oncology (COGNO). Phase 2 trial of temozolomide and pegylated liposomal doxorubicin in the treatment of patients with glioblastoma multiforme following concurrent radiotherapy and chemotherapy. *J. Clin. Neurosci.* **2011**, *18*, 1444–1448.

[12] Liu, Y. B.; Chen, L. G. Comparison of clinical effects of temozolomide single agent and combined doxorubicin in the treatment of glioma. *J. Healthc. Eng.* **2022**, *2022*, 7995385.

[13] Zhou, Y.; Wang, L.; Wang, C. J.; Wu, Y. L.; Chen, D. M.; Lee, T. H. Potential implications of hydrogen peroxide in the pathogenesis and therapeutic strategies of gliomas. *Arch. Pharm. Res.* **2020**, *43*, 187–203.

[14] Yasaswi, P. S.; Shetty, K.; Yadav, K. S. Temozolomide nano enabled medicine: Promises made by the nanocarriers in glioblastoma therapy. *J. Control. Release* **2021**, *336*, 549–571.

[15] Wang, X. Y.; Li, C.; Wang, Y. G.; Chen, H. B.; Zhang, X. X.; Luo, C.; Zhou, W. H.; Li, L. L.; Teng, L. S.; Yu, H. J. et al. Smart drug delivery systems for precise cancer therapy. *Acta Pharm. Sin. B* **2022**, *12*, 4098–4121.

[16] Zhang, Y. F.; Cheng, Q.; Xue, Y. H.; Yao, K.; Syeda, Z. M.; Xu, J.; Wu, J. H.; Wang, Z. J.; Tang, L. G.; Mu, Q. C. LAT1 targeted brain delivery of temozolomide and sorafenib for effective glioma therapy. *Nano Res.*, in press, https://doi.org/10.1007/s12274-023-5568-3.

[17] Batrakova, E. V.; Kim, M. S. Using exosomes, naturally-equipped nanocarriers, for drug delivery. *J. Control. Release* **2015**, *219*, 396–405.

[18] Kalluri, R.; LeBleu, V. S. The biology, function, and biomedical applications of exosomes. *Science* **2020**, *367*, eaau6977.

[19] Yong, T. Y.; Zhang, X. Q.; Bie, N. N.; Zhang, H. B.; Zhang, X. T.; Li, F. Y.; Hakeem, A.; Hu, J.; Gan, L.; Santos, H. A. et al. Tumor exosome-based nanoparticles are efficient drug carriers for chemotherapy. *Nat. Commun.* **2019**, *10*, 3838.

[20] Qiao, L.; Hu, S. Q.; Huang, K.; Su, T.; Li, Z. H.; Vandergriff, A.; Cores, J.; Dinh, P. U.; Allen, T.; Shen, D. L. et al. Tumor cell-derived exosomes home to their cells of origin and can be used as Trojan horses to deliver cancer drugs. *Theranostics* **2020**, *10*, 3474–3487.

[21] Zhang, X.; Zhang, H. B.; Gu, J. M.; Zhang, J. Y.; Shi, H.; Qian, H.;

Wang, D. Q.; Xu, W. R.; Pan, J. M.; Santos, H. A. Engineered extracellular vesicles for cancer therapy. *Adv. Mater.* **2021**, *33*, 2005709.

[22] Wang, A. Z.; Gu, F.; Zhang, L. F.; Chan, J. M.; Radovic-Moreno, A.; Shaikh, M. R.; Farokhzad, O. C. Biofunctionalized targeted nanoparticles for therapeutic applications. *Expert Opin. Biol. Ther.* **2008**, *8*, 1063–1070.

[23] Israel, L. L.; Braubach, O.; Galstyan, A.; Chiechi, A.; Shatalova, E. S.; Grodzinski, Z.; Ding, H.; Black, K. L.; Ljubimova, J. Y.; Holler, E. A combination of tri-leucine and angiopep-2 drives a polyanionic polymalic acid nanodrug platform across the blood-brain barrier. *ACS Nano* **2019**, *13*, 1253–1271.

[24] Zou, Y.; Sun, X. H.; Wang, Y. B.; Yan, C. N.; Liu, Y. J.; Li, J.; Zhang, D. Y.; Zheng, M.; Chung, R. S.; Shi, B. Y. Single siRNA nanocapsules for effective siRNA brain delivery and glioblastoma treatment. *Adv. Mater.* **2020**, *32*, 2000416.

[25] Zhu, Z. C.; Zhai, Y. X.; Hao, Y.; Wang, Q. W.; Han, F.; Zheng, W. L.; Hong, J.; Cui, L. S.; Jin, W.; Ma, S. C. et al. Specific anti-glioma targeted-delivery strategy of engineered small extracellular vesicles dual-functionalised by angiopep-2 and TAT peptides. *J. Extracell. Vesicles* **2022**, *11*, e12255.

[26] Singh, S. K.; Hawkins, C.; Clarke, I. D.; Squire, J. A.; Bayani, J.; Hide, T.; Henkelman, R. M.; Cusimano, M. D.; Dirks, P. B. Identification of human brain tumour initiating cells. *Nature* **2004**, *432*, 396–401.

[27] Cho, J. H.; Kim, A. R.; Kim, S. H.; Lee, S. J.; Chung, H.; Yoon, M. Y. Development of a novel imaging agent using peptide-coated gold nanoparticles toward brain glioma stem cell marker CD133. *Acta Biomater.* **2017**, *47*, 182–192.

[28] Wang, Z. H.; Sun, M. Q.; Li, W.; Fan, L. Y.; Zhou, Y.; Hu, Z. Y. A novel CD133- and EpCAM-targeted liposome with redox-responsive properties capable of synergistically eliminating liver cancer stem cells. *Front. Chem.* **2020**, *8*, 649.

[29] Wang, Y. H.; Jia, F.; Wang, Z. H.; Qian, Y. X.; Fan, L. Y.; Gong, H.; Luo, A. Q.; Sun, J.; Hu, Z. Y.; Wang, W. Z. Boosting the theranostic effect of liposomal probes toward prominin-1 through optimized dual-site targeting. *Anal. Chem.* **2019**, *91*, 7245–7253.

[30] Wang, W. Z.; Wang, Z. H.; Bu, X. L.; Li, R.; Zhou, M. X.; Hu, Z. Y. Discovering of tumor-targeting peptides using Bi-functional microarray. *Adv. Healthc. Mater.* **2015**, *4*, 2802–2808.

[31] Kamerkar, S.; LeBleu, V. S.; Sugimoto, H.; Yang, S. J.; Ruivo, C. F.; Melo, S. A.; Lee, J. J.; Kalluri, R. Exosomes facilitate therapeutic targeting of oncogenic KRAS in pancreatic cancer. *Nature* **2017**, *546*, 498–503.

[32] You, L. H.; Wang, J.; Liu, T. Q.; Zhang, Y. L.; Han, X. X.; Wang, T.; Guo, S. S.; Dong, T. Y.; Xu, J. C.; Anderson, G. J. et al. Targeted brain delivery of rabies virus glycoprotein 29-modified deferoxamine-loaded nanoparticles reverses functional deficits in parkinsonian mice. *ACS Nano* **2018**, *12*, 4123–4139.

[33] Tönjes, M.; Barbus, S.; Park, Y. J.; Wang, W.; Schlotter, M.; Lindroth, A. M.; Pleier, S. V.; Bai, A. H. C.; Karra, D.; Piro, R. M. et al. BCAT1 promotes cell proliferation through amino acid catabolism in gliomas carrying wild-type IDH1. *Nat. Med.* **2013**, *19*, 901–908.

[34] Di Tacchio, M.; Macas, J.; Weissenberger, J.; Sommer, K.; Bähr, O.; Steinbach, J. P.; Senft, C.; Seifert, V.; Glas, M.; Herrlinger, U. et al. Tumor vessel normalization, immunostimulatory reprogramming, and improved survival in glioblastoma with combined inhibition of PD-1, angiopoietin-2, and VEGF. *Cancer Immunol. Res.* **2019**, *7*, 1910–1927.

[35] Fang, R. P.; Chen, X.; Zhang, S. C.; Shi, H.; Ye, Y. Q.; Shi, H. L.; Zou, Z. Y.; Li, P.; Guo, Q.; Ma, L. et al. EGFR/SRC/ERK-stabilized YTHDF2 promotes cholesterol dysregulation and invasive growth of glioblastoma. *Nat. Commun.* **2021**, *12*, 177.

[36] Jiang, Y.; Yang, W. J.; Zhang, J.; Meng, F. H.; Zhong, Z. Y. Protein toxin chaperoned by LRP-1-targeted virus-mimicking vesicles induces high-efficiency glioblastoma therapy *in vivo*. *Adv. Mater.* **2018**, *30*, 1800316.

[37] Wang, W. Z.; Ma, Z. R.; Zhu, S. J.; Wan, H.; Yue, J. Y.; Ma, H. L.; Ma, R.; Yang, Q. L.; Wang, Z. H.; Li, Q. et al. Molecular cancer imaging in the second near-infrared window using a renal-excreted NIR-II fluorophore-peptide probe. *Adv. Mater.* **2018**, *30*, 1800106.

[38] Naghibi, S.; Sabouri, S.; Hong, Y. N.; Jia, Z. F.; Tang, Y. H. Brush-like polymer prodrug with aggregation-induced emission features for precise intracellular drug tracking. *Biosensors* **2022**, *12*, 373.

[39] Zhou, Y.; Guo, Y. X.; Chen, L. F.; Zhang, X. L.; Wu, W.; Yang, Z. M.; Li, X. J.; Wang, Y. Z.; Hu, Z. Y.; Wang, Z. H. Co-delivery of phagocytosis checkpoint and STING agonist by a Trojan horse nanocapsule for orthotopic glioma immunotherapy. *Theranostics* **2022**, *12*, 5488–5503.

[40] Zhao, Z.; Zhang, K. N.; Wang, Q. W.; Li, G. Z.; Zeng, F.; Zhang, Y.; Wu, F.; Chai, R. C.; Wang, Z.; Zhang, C. B. et al. Chinese Glioma Genome Atlas (CGGA): A comprehensive resource with functional genomic data from chinese glioma patients. *Genom. Proteom. Bioinf.* **2021**, *19*, 1–12.

[41] Qian, R. J.; Jing, B. P.; Jiang, D. W.; Gai, Y. K.; Zhu, Z. Y.; Huang, X. J.; Gao, Y.; Lan, X. L.; An, R. Multi-antitumor therapy and synchronous imaging monitoring based on exosome. *Eur. J. Nucl. Med. Mol. Imaging* **2022**, *49*, 2668–2681.

[42] Paskeh, M. D. A.; Entezari, M.; Mirzaei, S.; Zabolian, A.; Saleki, H.; Naghdi, M. J.; Sabet, S.; Khoshbakht, M. A.; Hashemi, M.; Hushmandi, K. et al. Emerging role of exosomes in cancer progression and tumor microenvironment remodeling. *J. Hematol. Oncol.* **2022**, *15*, 83.

[43] Guo, Y. H.; Hu, G. W.; Xia, Y. G.; Li, H. Y.; Yuan, J.; Zhang, J. T.; Chen, Y.; Guo, H.; Yang, Y. L.; Wang, Y. et al. Eliminating the original cargos of glioblastoma cell-derived small extracellular vesicles for efficient drug delivery to glioblastoma with improved biosafety. *Bioact. Mater.* **2022**, *16*, 204–217.

[44] Khan, I.; Baig, M. H.; Mahfooz, S.; Imran, M. A.; Khan, M. I.; Dong, J. J.; Cho, J. Y.; Hatiboglu, M. A. Nanomedicine for glioblastoma: Progress and future prospects. *Semin. Cancer Biol.* **2022**, *86*, 172–186.

[45] Zhao, M. N.; van Straten, D.; Broekman, M. L. D.; Préat, V.; Schiffelers, R. M. Nanocarrier-based drug combination therapy for glioblastoma. *Theranostics* **2020**, *10*, 1355–1372.

[46] Kim, J. S.; Shin, D. H.; Kim, J. S. Dual-targeting immunoliposomes using angiopep-2 and CD133 antibody for glioblastoma stem cells. *J. Control. Release* **2018**, *269*, 245–257.

[47] Guo, M. F.; Wu, F.; Hu, G. R.; Chen, L.; Xu, J. J.; Xu, P. W.; Wang, X.; Li, Y. M.; Liu, S. Q.; Zhang, S. et al. Autologous tumor cell-derived microparticle-based targeted chemotherapy in lung cancer patients with malignant pleural effusion. *Sci. Transl. Med.* **2019**, *11*, eaat5690.

[48] Villa, A.; Garofalo, M.; Crescenti, D.; Rizzi, N.; Brunialti, E.; Vingiani, A.; Belotti, P.; Sposito, C.; Franzè, S.; Cilurzo, F. et al. Transplantation of autologous extracellular vesicles for cancer-specific targeting. *Theranostics* **2021**, *11*, 2034–2047.

[49] Wang, Y. M.; Xu, X. Y.; Chen, X. Y.; Li, J. S. Multifunctional biomedical materials derived from biological membranes. *Adv. Mater.* **2022**, *34*, 2107406.

[50] Guo, X.; Sui, R.; Piao, H. Z. Tumor-derived small extracellular vesicles: Potential roles and mechanism in glioma. *J. Nanobiotechnol.* **2022**, *20*, 383.

[51] Ruan, S. B.; Greenberg, Z.; Pan, X. S.; Zhuang, P.; Erwin, N.; He, M. Extracellular vesicles as an advanced delivery biomaterial for precision cancer immunotherapy. *Adv. Healthc. Mater.* **2022**, *11*, 2100650.

[52] Zhang, Q. P.; Xu, B. C.; Chen, J. L.; Chen, F. R.; Chen, Z. P. Clinical significance of CD133 and Nestin in astrocytic tumor: The correlation with pathological grade and survival. *J. Clin. Lab. Anal.* **2020**, *34*, e23082.